Electronic properties of twin boundaries and twinning superlattices in diamond-type and zinc-blende-type semiconductors

Z. Ikonić, G. P. Srivastava, and J. C. Inkson
Department of Physics, Exeter University, Stocker Road, Exeter EX4 4QL, United Kingdom
(Received 9 July 1993)

The electronic properties of twinning boundaries, stacking faults, and a recently proposed structure, the twinning superlattice, in group IV and III-V diamond-type and zinc-blende-type semiconductors are calculated and discussed.

I. INTRODUCTION

With the advent of modern technologies of crystal growth, it has become possible to make high-quality semiconductor layered structures, with novel electronic properties. Of the most famous representatives of those, superlattices, two classes have traditionally been grown, based on periodic changes of either composition or doping patterns. For making high-quality compositional superlattices, the closeness of the lattice constants of constituent semiconductors is a prerequisite. When the lattice constants of the semiconductors differ by a finite amount, as is usually the case, great care has to be taken to obtain a good interface, which may involve rather complicated chemistry, tightly controlled growth conditions, etc. Failure to meet this condition results in a large number of defects and dangling bonds in the vicinity of the interface, thus degrading their electronic properties, due to the large amount of incoherent electron scattering introduced. This leaves a limited number of semiconductor materials for superlattice growth. Problems of a similar nature may also appear in the case of doping superlattices.

The periodic variation in material composition gives rise to miniband formation through the coherent admixture of states of the constituent materials. In the case of the doping superlattice, it is the coherent scattering due to the periodic electrostatic potential which performs the same function. However, a spatially varying potential is not the only way to introduce electron scattering in semiconductors. The possibility also exists to make a single semiconductor material behave as an inhomogeneous structure. This can be done in at least two other ways, as follows.

Some semiconductors naturally show polytypism, i.e., the face-centered-cubic (fcc) and hexagonal-close-packed (hcp) crystalline forms may coexist, because the formation energies of the two phases differ by a very small amount (SiC and ZnS being typical examples). A considerable amount of work has been done on these systems, and the formation energies, as well as electronic and other properties of these structures, have been rather thoroughly studied.[1–5] In such materials the fcc and hcp phases may be interleaved, so as to make a rather long period unit cell. It is thus possible to conceive of polytype (or heterocrystalline) superlattices, which show a specific polytypic sequence of the constituent semiconductor, containing both fcc and hcp portions of the same material, periodically repeated. Polytype superlattices were studied within simple models some time ago,[6] and interest in them was very recently renewed,[7] with the use of more sophisticated methods of calculation.

Viewed as a periodic stack of layers with different crystal structures, such systems introduce electron scattering at interfaces and the formation of superlattice states, because the Bloch wave functions in the two adjacent layers are quite different. We should note, however, that many of the properties of this kind of superlattice may still qualitatively be understood and treated by simple effective-mass methods, since fcc and hcp phases have, *inter alia,* different band gaps. Indeed, such an approach has been adopted in Ref. 6. It is also important to note that although the two crystal phases are different, they are essentially perfectly lattice-matched at the interface, and all the bonds are preserved.

Another method of introducing periodic "scattering centers" in a semiconductor is to vary the crystal orientation. To be useful, this has to be done in such a way that no stress and/or dangling bonds appear at the interface of the two differently oriented semiconductors. These ideas bring us to the field of a class of planar defects in semiconductor crystals, known as stacking faults, that we shall first briefly discuss.

Stacking faults are one of the most common types of defects in crystalline diamond-type and zincblende-type semiconductors (Si, Ge, GaAs,...), as well as in many face-centered-cubic metals. They are created when changes of the atomic plane stacking sequence in the [111] direction, as compared to the perfect crystal, take place, without breaking any bonds, and have very low formation energies. The most elementary stacking fault, which is at the same time the building block for all other types, is the twin stacking fault (or twin boundary, 180° twist boundary). It comprises the reversal of the stacking sequence at some plane, i.e., instead of the $AA'BB'CC'AA'BB'CC'$ sequence of the perfect crystal, one now has

$$AA'BB'CC'A|A'CC'BB'AA' ,$$

where AA' (or BB',CC') denote the two basis atoms of the primitive unit cell. Formally, a twin stacking fault can be constructed by cutting the [111] directed bonds in,

say the AA' layer, rotating half of the crystal at 180° about the bond axis and then reconnecting all cut bonds of two crystal halves. The junction of the two crystal halves is perfect in the sense that all the bond lengths and angles are preserved and no dangling bonds are generated. The other two common types of stacking faults are intrinsic and extrinsic, having one missing or one extra layer, respectively, in an otherwise unperturbed crystal. Thus, along the [111] direction the intrinsic and extrinsic stacking faults have the stacking sequences

$$AA'BB'CC'\|BB'CC'AA'BB'$$

and

$$AA'BB'CC'|BB'|AA'BB'CC' ,$$

respectively. They may also be viewed as two twin stacking faults separated by one (intrinsic) or two (extrinsic) atomic bilayers of reversely oriented material (note that one monolayer of a zinc-blende crystal has two atoms, as mentioned above).

The essentials of the physics of the stacking fault that we exploit is that although the interface between the two crystal orientations is perfectly lattice-matched, the wave functions are highly symmetry-mismatched. This makes the twin stacking fault in a sense a junction of two essentially *different* materials, even though the material is of the *same* composition and lattice type on both sides. This symmetry mismatch must give rise to rather large electron scattering at the interface, and it has indeed been observed in single stacking faults, especially for energies not so high above the band edge.[8,9]

Stacking-fault defects in semiconductors usually occur unintentionally, e.g., due to strain. They can have a considerable effect on bulk semiconductor devices, acting, e.g., as scattering centers and lowering the electron mobility, or as recombination centers, etc. However, stacking faults may also be produced intentionally.

We have recently proposed a superlattice, namely the twinning superlattices,[10] based upon the concept of a periodic combination of two differently oriented semiconductors. Thus, twinning superlattices would comprise periodic reversal of atomic stacking sequence, i.e., periodically distributed twin boundaries, in a semiconductor which is otherwise, in terms of material composition or doping, homogeneous. Limited efforts seem to have been directed towards the fabrication of various stacking faults, and the most important report on growing a high-quality, possibly large-area, single twin boundary, has appeared quite recently.[11] In this experiment, by depositing a submonolayer of boron during the molecular beam epitaxy (MBE) growth of silicon, Headrick *et al.* were able to incorporate in it an essentially perfect plane stacking fault. In view of this successful growth of a single twin boundary in Si, fabricating a superlattice structure now seems quite feasible.

Given the two possible orientations of the constituent diamond-type or zinc-blende-type semiconductor (if the interface is to remain perfect), one period of a twinning superlattice, in its simplest version, might include n and m atomic bilayers of oppositely oriented material. (Of course, more complicated structures are also possible, where the two crystal orientations are distributed over a number of alternating layers within the superlattice period.) Among the general (m,n) twinning superlattices, special cases (n,n), $(n,1)$ with $n>1$, and $(n,2)$ with $n>2$ may, in accordance with the existing terminology for isolated stacking faults, be called the twin, intrinsic, and extrinsic stacking-fault superlattices, respectively.

The proposed twinning superlattices can be readily distinguished from the polytype superlattices discussed previously. In twinning superlattices no change of the underlying crystal structure is involved: it is only the crystal orientation that alternates periodically. In view of the fact that the class of crystals allowing for twinning[12] is much larger than the class of crystals showing polytypism, there is, in principle, a considerably wider choice of materials for making twinning superlattices than there is for polytype superlattices. Except in SiC and (Zn,Cd)(S,Se), where even "natural" superlattice structures may appear,[6] polytypism is not expected to be a frequently found phenomenon, because fcc and hcp energies usually differ too much.[2] On the other hand, a wide variety of crystals show twinning, which is enabled by the crystal symmetry,[12] not its composition, and indeed it may be found in a large number of minerals.[13,14] In this paper, however, we concentrate only on diamond- and zincblende-based twinning superlattices.

The recent success in the growth of a single twin boundary in silicon[11] indicates the potential for fabrication of twinning superlattices. However, we are not presently aware of any attempt in this direction. Interestingly, twinning superlattices are the only type of superlattice structures that may be found among natural minerals. In mineralogy they are known as polysynthetic twins and may appear in a number of (unfortunately insulating, not semiconducting) crystals, notably the plagioclase feldspars, such as albite.[13] In natural specimens the periodicity may not be perfect, and layers are wider than is usual in the field of quantum microstructures, but they still exhibit interesting optical effects.[13] Also worth mentioning is that pure single crystals of calcium mesodigermanate, laboratory grown from melt, display regular twinning,[15] constituting an "unintentionally" made twinning superlattice. The possibilities of fabricating such structures will be further discussed in more detail in Sec. IV.

In this paper we first analyze the electronic properties of single stacking faults in a few of diamond-type and zincblende-type semiconductors (Si, Ge, GaAs, AlAs), thus somewhat extending the work of previous authors to different semiconductors. We then calculate and discuss the electronic properties of twinning superlattices, based on these four semiconductors.

II. THE METHOD AND SOME PHYSICAL CONSIDERATIONS

As discussed in the Introduction, any stacking-fault structure comprises at least one planar defect, i.e., the junction of two misoriented crystal halves. The 180° ro-

tation used to make the twin boundary has nontrivial consequences on the stacking-fault electronic structure. However, many of these cannot be understood within the "continuum" models, such as the effective-mass method, because neither the potential nor the effective mass change across the boundary, and these techniques do not explicitly recognize the cell-periodic part of the wave function. Only the more sophisticated, microscopic methods that do may be used for this purpose, e.g., empirical pseudopotential, tight-binding, *ab initio* pseudopotential, and similar techniques.

All calculations[8,9,16–23] performed on stacking faults in semiconductors until now have been exclusively for silicon. Most have considered their formation energy, phonon spectra, and the existence of interface bound states, while a few[8,9] have dealt with electron transmission through them. There is also a number of papers on stacking faults in face-centered-cubic metal crystals (e.g., Refs. 24–26) such as Al and Cu, most of which dealt with their formation energy and mechanical properties, but not electronic properties (with the noteworthy exception of Ref. 24, where the electron transmission through stacking faults in copper was calculated).

In the well-studied case of stacking faults in silicon, both the empirical-pseudopotential[16–18] and more sophisticated self-consistent methods of various types[8,19–21] have been employed. Results of these two classes of calculations show a remarkable degree of mutual agreement. The formation energy of the intrinsic stacking fault in Si (55 erg/cm^2) calculated in Ref. 16, for instance, is within the spread of values given in Refs. 19–21 (33–145 erg/cm^2), and incidentally is closer to the experimental data, although the charge redistribution and lattice relaxation were ignored. Similarly, energy locations of the interface states above the valence-band and below the conduction-band edges at the center of the Brillouin zone calculated by all these methods[8,17–21] do not differ very much. In the case of the interface state in the vicinity of the conduction-band X-valley bottom, however, disagreements on its existence and energy location do appear, but they seem to be uncorrelated with the sophistication of the method and probably reflect the sensitivity of this state to the parameters used. Self-consistent calculations[19–21] of atomic relaxation and charge redistribution in stacking faults show that these effects are not very strong, and thus do not have a great deal of influence on their electronic properties. This can be understood when one remembers that the nearest-neighbor surrounding in stacking faults is just the same as in perfect crystals, with differences appearing in the next-nearest neighbors only. With this in view, we employed in our calculations the empirical pseudopotentials, which describe the eigenstates and energy bands of the semiconductor quite well. Our method should be adequate for the purpose of calculating electronic properties of stacking faults, and superstructures based upon them, with reasonable accuracy. Even though quantitative discrepancies might be expected if more elaborate schemes were used, the empirical-pseudopotential-based method, as discussed above, should reveal all the major physical effects and their trends.

A. Details of the calculations

The method used in our calculations is an empirical-pseudopotential-based layer method.[27] It uses the bulk band-structure data to find properties of more complex (micro)structures. Basically, we first calculate the complex band structure and eigenfunctions of both the propagating and evanescent states of the two bulk semiconductors on either side of the interface. The in-plane ($\mathbf{g}_\parallel$) Fourier components of the eigenfunctions are then matched at the interface(s) and functions propagated along the layers. The wave-function propagation and matching is performed using the S-matrix approach, which guarantees high stability against the evanescent states (see Ref. 27 for details).

Thus, this method does not belong to the class of supercell methods. All the results obtained within it are subject to interpretation via the bulk band-structure concepts. Yet, along with the advantage of simplicity, such a calculation may be expected to reveal all the band-structure-related properties of single stacking faults and twinning superlattices arising from band mixing and bulk Brillouin zone folding. It is only the possible charge redistribution around the interface that would remain undescribed, but, as mentioned above, this is not expected to be very significant.[19–21]

For the interface between two different materials, the set of wave functions and their derivatives at a given energy (E) and parallel wave vector ($\mathbf{k}_\parallel$) on either side are matched across the whole planar interface. In effect, this corresponds to matching the components at each lattice vector of the surface reciprocal lattice ($\mathbf{g}_\parallel$). For a twin boundary the materials are the same but of a different orientation. Thus, in practice, with an incident-electron state specified by its transverse wave-vector $\mathbf{k}_\parallel$ value, eigenfunctions on one side are calculated in the conventional way, and to obtain the eigenfunctions for the oppositely oriented material, the calculation is repeated for $\mathbf{k}_\parallel \rightarrow -\mathbf{k}_\parallel$ (but with the same "normal" crystal orientation) and then $\mathbf{g}_\parallel$ and $-\mathbf{g}_\parallel$ components of the wave function are interchanged. The matching then proceeds in the usual manner.[27]

Calculation of the twinning-superlattice miniband structure goes along the lines described in our earlier paper.[28] In brief, the S matrix of a superlattice period is first calculated, taking advantage of the high stability of the technique. Upon finding the full S matrix, it is recast into the T matrix, the Bloch conditions are imposed, and the eigenequation is solved.

B. Electron behavior at the twin boundary

In order to get a physical insight, within the framework employed, in the phenomena occurring at the twinning boundary and related structures based on it, we shall first give a brief description of relevant bulk band-structure details. The first Brillouin zone of bulk IV and III-V semiconductors is the well-known truncated octahedron, depicted in Fig. 1, with the important points, Γ, X, and L also denoted. When a bulk crystal is rotated, the first Brillouin zone corresponding to it (albeit in $\mathbf{k}$

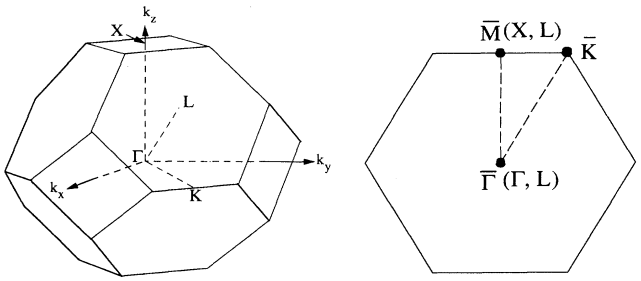

(a) Bulk BZ (b) Interface BZ

FIG. 1. The first Brillouin zone of the zinc-blende lattice (left) and the (111) interface Brillouin zone with mapping of some important points of the bulk Brillouin zone denoted (right).

space) also rotates, since both the real and **k** spaces are "tied" to the same coordinate system. In many cases this rotation has no physical significance whatsoever, but in the case of twinning stacking faults, or more complex structures of this type, the situation is different: just as the two crystal halves are rotated *relative* to each other, the same holds true for their Brillouin zones. The first Brillouin zone is not mirror symmetric with respect to the (111) plane, which has important consequences on the coupling of various bulk states at the twin boundary (interface).

In order to get some insight into the state coupling and mixing involved, it is useful to relate the bulk Brillouin zone points (especially the low-energy ones, Γ, X and L) to points of the interface Brillouin zone, also given in Fig. 1. The bulk Brillouin zone points Γ and two out of the eight L (those "directed" along the [111] and $[\bar{1}\bar{1}\bar{1}]$ directions, symmetrically situated with respect to Γ) are projected onto $\bar{\Gamma}$, while all the six X, and six "tilted" L points (in pairs, one of each kind) project onto six $\bar{M}$ points of the interface Brillouin zone. Therefore, $\bar{\Gamma}$ and $\bar{M}$ are the most important $\mathbf{k}_{\parallel}$ points of the interface Brillouin zone to be explored (Fig. 1).

Upon 180° rotation in real space, the wave functions and band structure at any general $\mathbf{k}_{\parallel}$ point change, following the real-space crystal structure. The exception to this rule is the dispersion along the [111] line passing through the Γ point, which, being symmetric, remains unchanged. However, even here the transverse structure of the wave function in the [111] plane is not invariant under the 180° rotation. At any one of the six equivalent $\bar{M}$ points, the bulk band structure is asymmetric, due to unequally situated X and L valleys with respect to the [111] plane. Specifically, taking an X and an L valley that are projected to the same $\bar{M}$ point, if the L valley is at k_L, then the X valley is at $k_X=-2k_L$ away from the [111] plane ($[k_L=\pm(1/2\sqrt{3})](2\pi/a)$, a is the cubic lattice constant), the sign depending on the particular $\bar{M}$ point chosen. In the two oppositely oriented crystal halves on either side of the twin boundary (call them a and b), the signs of k_L and k_X at the same $\bar{M}$ point are reversed. Consequently, the X (L) states on the opposite sides are really different states, say X_a and X_b (L_a and L_b), since they arise from two different valleys. There is no direct match for the X_a state in the b layer, and vice versa, just as at the junction of two completely different crystal structures.

For the above reasons a considerable scattering and/or band mixing may be expected to occur at the twin boundary, clearly much more so at the $\bar{M}$ than at the $\bar{\Gamma}$ point. Also, the band mixing is expected to be more pronounced here than in the conventional heterostructures, such as GaAs/AlAs, where the wave functions in the two layers are "symmetry similar," because the two semiconductors are crystallographically aligned. Certainly, mixing is generally favored by the proximity of energy of the relevant states involved.

III. RESULTS

Numerical calculations of the electronic properties have been performed using the empirical-pseudopotential form factors from Refs. 29, 30, and 31 for Si, Ge, and (Ga,Al)As, respectively. Only the conduction-band states have been considered, and no spin-orbit interaction has been included (calculation of the valence-band properties will be performed at a later stage). As the results for the stacking faults and twinning superlattices are directly interpreted in terms of bulk band structure, it is important to have reasonably accurate results for the bulk. With the above form factors, the L valley in Si is 1 eV above X, and Γ is another 1 eV above L. Furthermore, at the exact X point the X_1 and X_3 states are degenerate, but at the X_1 valley minimum—the bottom of the conduction band—it is 460 meV below X_3 [this happens at $\mathbf{k}_{\parallel}=0.87\mathbf{k}_{\parallel}(\bar{M})$]. In Ge the X valley is only 180 meV above L, and Γ is 280 meV above L. GaAs, the only direct-band-gap semiconductor among the four studied, has its L and X valleys 320 and 490 meV above Γ, and, finally, in AlAs the L and Γ valleys are 280 and 600 meV, respectively, above the X valley. These are well within the results of other calculations and experiments (in any case, the main features of our results are independent on precise positions of the minima). With these values of conduction-band edges, band mixing is obviously likely to be more important in stacking faults and twinning superlattices based on Ge, GaAs, and AlAs, rather than in Si where various conduction-band extrema are widely separated.

In the pseudopotential layer method we used a total of 19 in-plane Fourier components ($\mathbf{g}_{\parallel}$ values) in interface matching, corresponding to a total of 59 three-dimensional (3D) reciprocal-lattice vectors, up to and including the (222) star. Some critical points were also tested with 31 $g_{\parallel}$ values [the equivalent of 89 3D vectors, including the (331) star], and no significant difference could be detected.

A. Isolated stacking faults

1. Electron transmission

In calculating the electron transmission, the incident state energies were taken in a limited range, starting from

the conduction-band edge at the corresponding point of the interface Brillouin zone, up to 200–300 meV above it, to cover the range that thermal or hot electrons normally acquire. The results for the electron transmission through a twin, intrinsic, and extrinsic stacking fault at $\bar{\Gamma}$ and $\bar{M}$ interface Brillouin-zone points are given in Figs. 2(a)–2(d). In all cases where there is just one valley in the energy range displayed, the others being well away, the transmission versus incident energy dependence is reasonably smooth for all the three structures. Intrinsic and extrinsic stacking faults are essentially two closely coupled twin boundaries. It can be seen that although there is certainly (geometrical) interference of waves scattered from the two interfaces,[9] their wavelengths are much too long to bring about any fast modulation of the transmission if only one valley is involved. On the other hand, in the case of closely spaced valleys, the interplay of intervalley and geometrical interference effects produces severe modulation of the transmission coefficient. Specifically, Ge and GaAs are very prominent examples of this latter type of behavior. At the $\bar{M}$ point their L and X valleys are quite close, and Figs. 2(c) and 2(d) indicate that the L-X mixing at the interface is very strong indeed (in accordance with the physical considerations given in Sec. II). An important point to note, with respect to the discussion of twinning-superlattice band structure presented later in this section, is that this mixing appears to be strong in the energy range where one of the two states is evanescent and the other propagating. In contrast, the Γ-L mixing at the $\bar{\Gamma}$ point (Fig. 2) is rather weak even in Ge, where Γ and L valleys are closest to each other.

If the incident state is not the bulk Γ state, then the transmission rises comparatively slowly with energy and the transmission of low-energy electrons is very poor. However, the Γ state with energy in excess of a couple of meV is very well transmitted (a consequence being that stacking faults hardly have any impact on electron transport in GaAs). Being highly symmetric, both in terms of its position in the interface Brillouin zone and its wavefunction transverse structure, the bulk Γ state is obviously least affected by the rotation of one-half of the crystal with respect to the other.

2. *Interface bound states and resonance*

We have made calculations for all $\mathbf{k}_{\parallel}$ points along the $\bar{\Gamma}$-$\bar{M}$ line of the interface Brillouin zone in search for the existence of interface bound states and/or resonances in all the three types of stacking faults. The results are given in Figs. 3(a)–3(d). Bound states and resonances are found to be entirely related to L valleys, and tend to be some tens of meV below the L valley edge at the corresponding $\mathbf{k}_{\parallel}$ point. They are almost purely L in character, the admixture of other bulk states being very low.

We did not find either bound states or resonances close to the interface Brillouin-zone edges in contrast to Stiles and Hamann,[8] who found resonance states in Si at the $\bar{M}$ point. This is not a result of the limited basis set used, but may be related to the method [Stiles and Hamann

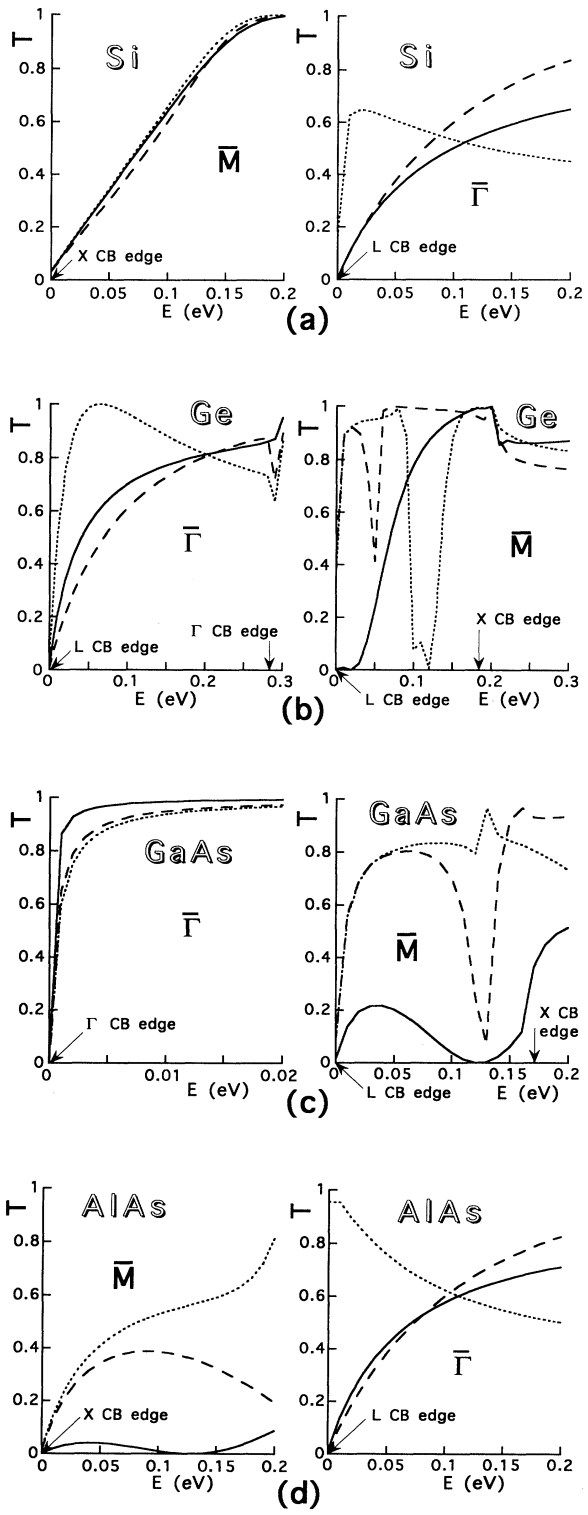

FIG. 2. Electron transmission coefficient vs incident electron energy for twinning (solid lines), intrinsic (long-dashed lines), and extrinsic (short-dashed lines) stacking faults at $\bar{\Gamma}$ and $\bar{M}$ interface Brillouin-zone points, for (a) Si, (b) Ge, (c) GaAs, and (d) AlAs. In all cases energy is measured from the *local* conduction-band edge at either the $\bar{\Gamma}$ or the $\bar{M}$ point (their absolute positions are different, except in Ge).

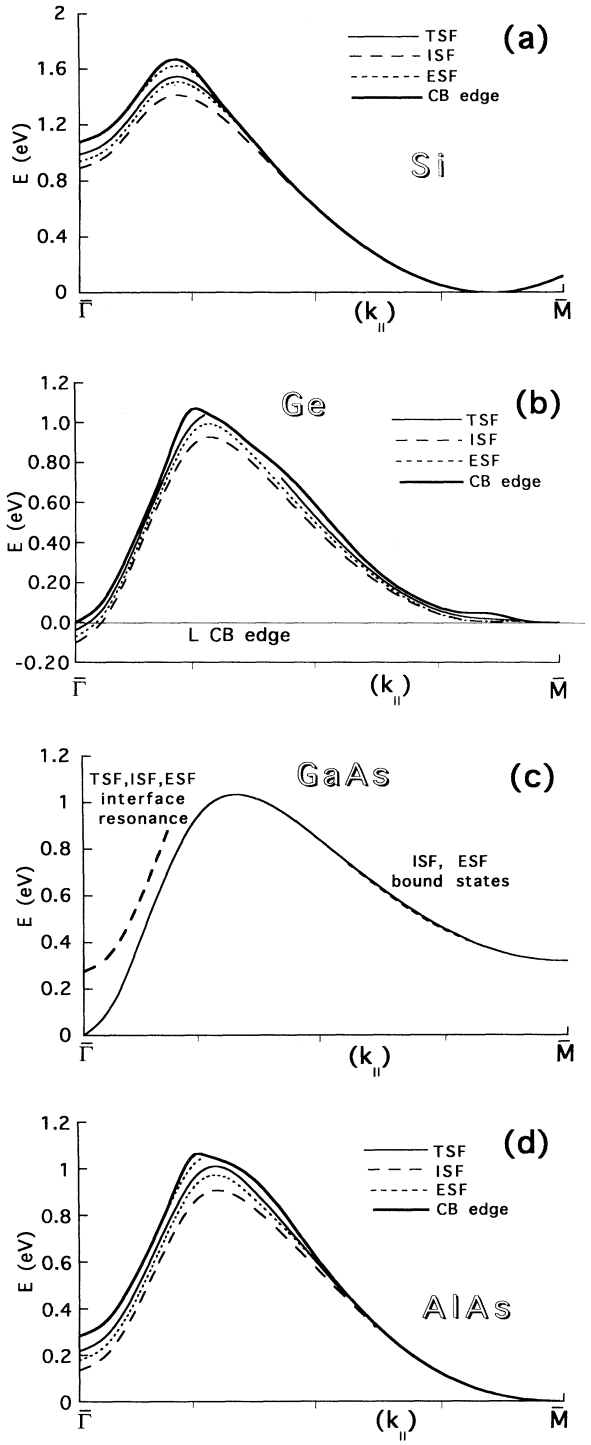

FIG. 3. Interface bound states and/or resonances along the $\bar{\Gamma}$-$\bar{M}$ line of the interface Brillouin zone (Fig. 1) for twinning (thin solid lines), intrinsic (long-dashed lines), and extrinsic (short-dashed lines) stacking faults in (a) Si, (b) Ge, (c) GaAs, and (d) AlAs. The heavy solid line denotes the conduction-band edge, as seen from the appropriate $\mathbf{k}_{\parallel}$ point along the $\bar{\Gamma}$-$\bar{M}$ line. (The $\bar{M}$ point is at $|\mathbf{k}_{\parallel}|=0.8165\cdot 2\pi/a$ away from the $\bar{\Gamma}$ point.) Note that the GaAs interface resonance is at the same energy for all three types of stacking faults.

used the linearized-augmented plane-wave (LAPW) density-functional theory] or with the definition of what constitutes a resonance state. At the $\bar{\Gamma}$ point, however, we did find a bound state in the Si twin stacking fault at precisely the same energy as Stiles and Hamann, i.e., 90 meV below the local conduction-band edge. An *ab initio* calculation by Chou, Cohen, and Louie,[21] with lattice relaxation and charge redistribution taken into account, however, gives a value of $\sim$200 meV for the state at $\bar{\Gamma}$, and also a real bound state somewhat below the conduction-band edge at the $\bar{M}$ point. The agreement between these results, with various uncertainties involved in the three computational schemes, may be considered as acceptable.

In Ge, where the L valley is the lowest at both $\bar{\Gamma}$ and $\bar{M}$ points of the interface Brillouin zone, bound states could be tracked from $\bar{\Gamma}$ almost up to $\bar{M}$, but finally disappeared. In contrast, in AlAs and Si, which are both the X-type indirect-gap semiconductors, bound states exist along a part of the $\bar{\Gamma}$-$\bar{M}$ line, until the point where the L valley comes in the "shadow" of the X valley. The L valley in Si, Ge, and AlAs is below Γ at $\bar{\Gamma}$, so real bound states could be found. In GaAs, however, the Γ valley is the lowest one, and here a strong interface resonance above the Γ valley, but below the L valley, was found. In spite of being predominantly L in character, the bound state is weakly coupled to the Γ continuum it is immersed in, and so forms a strong interface resonance.

As a single twin boundary is capable of supporting bound states, the presence of two interfaces (in intrinsic and extrinsic stacking faults) makes the two bound states interact in the conventional textbook manner, to form a symmetric and antisymmetric pair. In the extrinsic stacking fault, where the two interfaces are spaced by two crystal monolayers, we indeed found a pair of bound states in Si and AlAs, one above and the other below the twin stacking-fault bound-state energy. In an intrinsic stacking fault, however, the interfaces are closer and interaction between the states much stronger, so only the lower of them remains bound. The upper state seems to be pushed into the continuum, which is also L in character, making it completely disappear, or at most remain as a very weak, hardly detectable resonance (in the case of Ge, this applies to the extrinsic stacking fault as well). The interface resonance in GaAs, on the other hand, turns out to be independent of the structure—all three stacking faults considered have just one resonance state at exactly the same energy [Fig. 3(c)]. Interestingly, intrinsic and extrinsic stacking faults, but not a single twin stacking fault in GaAs, have bound states in a limited range of $\mathbf{k}_{\parallel}$ values approximately midway between the $\bar{\Gamma}$ and $\bar{M}$ points, well away from any of its valleys. However, their energies are so high that it is unlikely that they are of any importance.

B. Twinning superlattices

In this section we consider the electronic structure of twinning superlattices. Calculations were performed for the $\bar{M}$ and $\bar{\Gamma}$ points of the interface Brillouin zone only, since it is only here that the low-energy part of the miniband spectrum is to be expected. As discussed in Sec. II,

the miniband structure will be determined by both the interface scattering and band mixing. Since Si has widely separated conduction-band valleys, it allows one to identify clearly the effects of electron interface scattering, because the influence of intervalley mixing at the interface should be comparatively low. We therefore first consider the Si-based twinning superlattices and then compare with the results for other three semiconductors.

1. $\bar{M}$ point

The miniband electronic structure of Si-based $(n,1)$ intrinsic, and $(n,2)$ extrinsic stacking-fault superlattices, for $\mathbf{k}_{\parallel}$ corresponding to the local (and global) X-valley minimum, close to the $\bar{M}$ point of the interface Brillouin zone, is displayed in Figs. 4(a) and 4(b). The energy of the lowest miniband is significantly elevated from the conduction-band edge, which is consistent with poor transmission at low energies [Fig. 2(a)]. The positions of miniband edges in the superlattice Brillouin zone, also denoted in Fig. 4, vary with the superlattice structure, and always lie off the Brillouin-zone center or edges. Also displayed in Fig. 4 is the composition of various superlattice states, in terms of the contribution of various bulk states to the intensity of the wave function. A remarkable point is that the bulk X_3 and L states, though remote and thus evanescent, are rather highly excited, which is clearly due to the symmetry mismatch at the interface.

Now consider the miniband structure of the (n,n) twin stacking-fault superlattices, with $n=1\div 8$, displayed in Fig. 5(a). Miniband energies and the amount of intervalley mixing are about the same as in the two cases considered above. A distinct feature to note here is the occurrence of zero energy gaps at the superlattice Brillouin-zone boundary, i.e., pairs of minibands are joined back-to-back at $K_{\mathrm{SL}}=\pm\pi/d$ [where $d=(m+n)a/\sqrt{3}$ is the superlattice (SL) period] but are separated by a finite gap at $k_{\mathrm{SL}}=0$. Zero energy gaps ac-

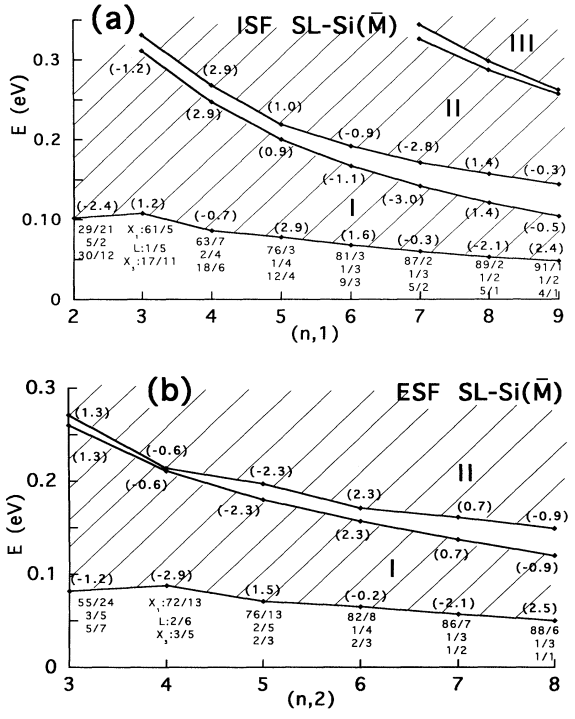

FIG. 4. Allowed minibands in (a) Si-based $(n,1)$ intrinsic and (b) $(n,2)$ extrinsic stacking-fault superlattices, close to the $\bar{M}$ point (the bulk X-valley bottom), from which the energy is measured. The solid lines connect miniband edges. Points of miniband extrema in the superlattice Brillouin zone (in $-\pi\le k_{\mathrm{SL}}d\le\pi$ units) are given in parentheses. The composition of the superlattice state at the lowest miniband bottom is also given. (The notation is the following: e.g., $X_1{:}z1/z2, L{:}z3/z4, \ldots$ means that, out of the total wave function squared in a superlattice period, $z1\%$ is the bulk X_1 state contribution in the first layer—the one with n atomic bilayers— and $z2\%$ in the second layer, with one or two atomic bilayers, etc. Thus all z's should add up to 100%, since states other than X_1, L, and X_3 turn out to give negligible contributions.)

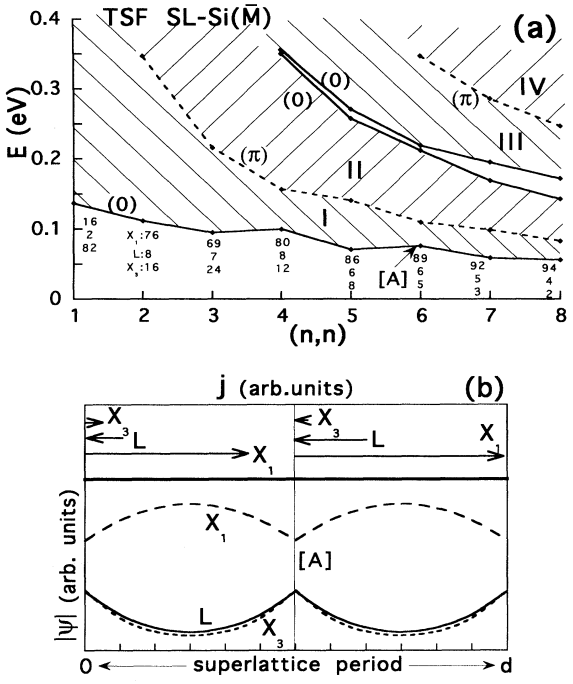

FIG. 5. (a) Same as Fig. 4, but for the Si (n,n) twin stacking-fault superlattice. Note the existence of zero energy miniband gaps, connected by dashed lines. Since the wave function at the miniband bottom is now evenly distributed among the layers, only the overall contribution of bulk states is displayed. (b) Envelope wave functions (lower part) and current j components (upper part) resolved into bulk L, X_1, X_3 contributions at point $[A]$ of (a), close to the first miniband edge (solid, dashed, and dotted lines, respectively, denote the wave-function components, and the current components, being piecewise constant, are proportional to the lengths of the arrows). The vertical lines denote twinning interfaces within the superlattice period, and the ticks along the horizontal axis denote the atomic bilayers.

tually occur not only at $\bar{M}$, but in fact at any general $\mathbf{k}_{\parallel}$ point of the interface Brillouin zone, and are a manifestation of the screw symmetry characterizing the unit cell (period) of this type of superlattice. Among all (m,n) twinning superlattices, and any other type of superlattices, the (n,n) twin stacking-fault superlattice is unique in that it possesses the screw symmetry, i.e, the translation by $d/2$ and rotation by 180°, both with respect to the superlattice axis, applied together leave the structure unchanged. It is well known from group theory that the screw symmetry leads to zero gaps at the Brillouin-zone edges.[32] Zero energy gaps of a different, physically significant nature may also be found in conventional superlattices, especially the effective-mass ones,[33] and are then usually restricted to some specific values of electron transverse wave vector, i.e., points in the interface Brillouin zone.

The plot of the envelope of the wave functions, given in Fig. 5(b), indicates that the X_1 state dominates, as expected, but contributions from X_3 and L states are again not

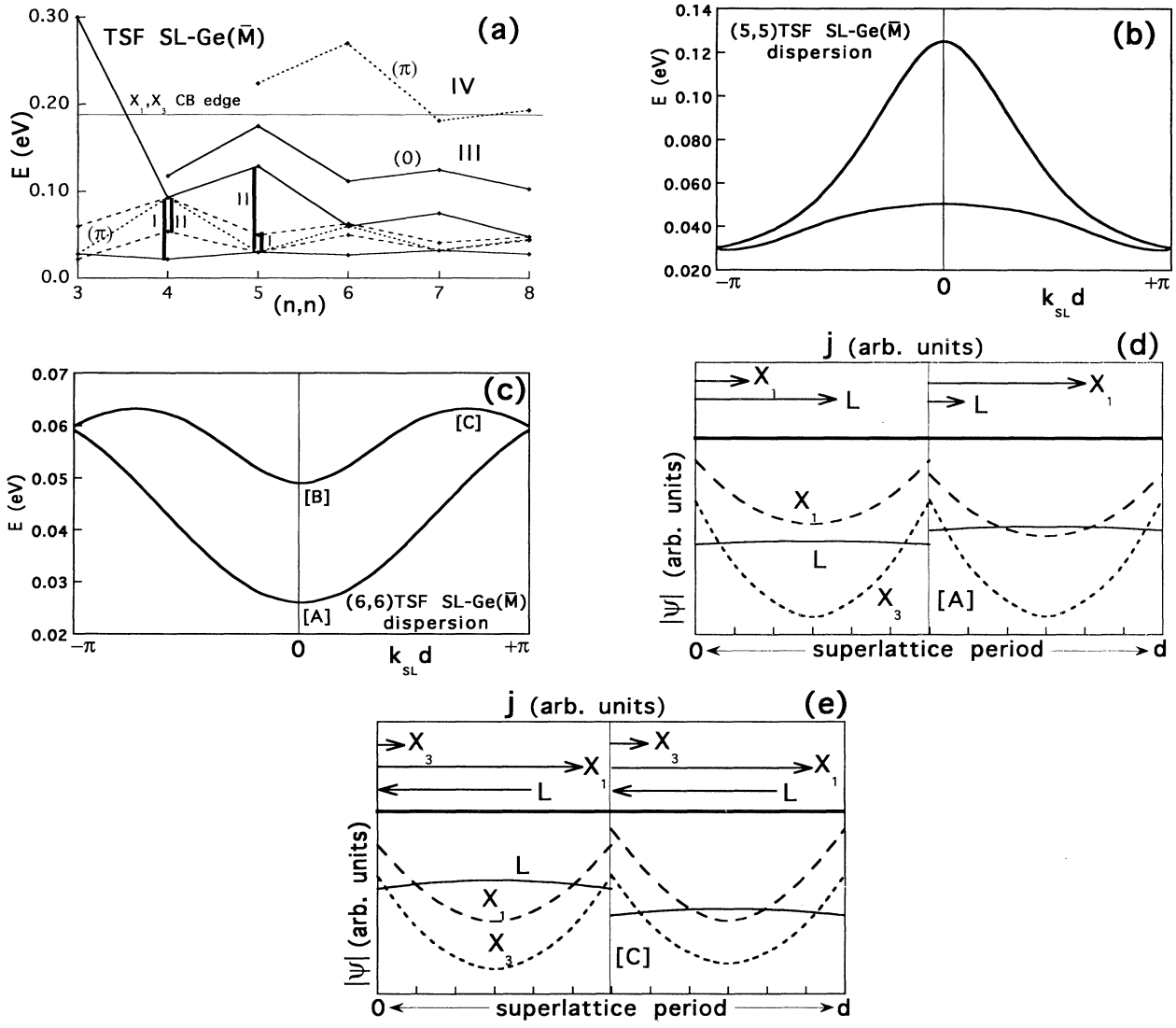

FIG. 6. (a) Miniband structure of the Ge-based (n,n) twin stacking-fault superlattice at the $\bar{M}$ point of the interface Brillouin zone. The energy is measured from the conduction-band edge at $\bar{M}$, which coincides with the bulk L-valley bottom. The solid lines connect the edges of minibands with normal dispersion, dashed lines those with "anomalous" dispersion, and dotted lines connect the zero energy gaps, at $k_{SL}=\pi/d$. Examples of energy ranges spanned by the lowest two minibands in (4,4) and (5,5) superlattices are also given, represented by heavy vertical bars. Unlike the first two, the third miniband behaves normally, beginning at $k_{SL}d=0$, ending at π (in brackets). (b,c) Dispersion of the lowest two minibands in Ge (5,5) and (6,6) twinning superlattices. (d,e) Envelope wave functions and current components resolved into bulk L, X_1, X_3 contributions [solid, dashed, and dotted lines, respectively, for the wave function, and arrows for the current, as in Fig. 5(b)], calculated at points [A] and [C] in the (6,6) superlattice above, the situation at [B] being quite similar to that at [A].

negligible. The same applies to current components (calculated slightly off the exact miniband extrema).

Calculations of the electronic structure of Ge-based twinning superlattices show that they share a few common features with Si-based ones, but also display some remarkable differences, to an extent that is almost qualitative. These differences clearly stem from the fact that valleys, L, X_1, and X_3 are much closer to each other in Ge than is the case in Si, and all contribute to the superlattice state.

The electronic structure of Ge-based (n,n) twin stacking-fault superlattices at the $\bar{M}$ point, shown in Fig. 6(a), is significantly different from the one in Si. On an energy scale it appears to have "embedded," or "overlapped," minibands [Fig. 6(a)]. A closer look at the miniband dispersion [Figs. 6(b) and 6(c)], however, reveals that pairs of minibands, one with normal and the other with "anomalous" dispersion, are joined (via zero energy gaps) at the superlattice Brillouin-zone edges (the term "anomalous" denoting comparatively low dispersion, with a local extremum somewhere inside the superlattice Brillouin zone). In the unfolded zone picture, allowing for the screw symmetry, the miniband dispersion has local extrema not only at the superlattice Brillouin-zone center and edges, but also at some inner points. Of the two adjacent minibands, it is the lower one that has anomalous dispersion for (odd,odd), and the higher one for (even,even) superlattices [cf. Figs. 6(b) and 6(c)]. The effect of anomalous dispersion disappears at higher energies, and minibands III and IV in Fig. 6(a) behave normally, as in Si. The corresponding calculations performed for GaAs and AlAs (not displayed) show that this is related to energy, rather than to the miniband index.

The wave-function plots at some characteristic points, displayed in Figs. 6(d) and 6(e) are generally similar to those in Si, but with grossly enhanced intervalley mixing effects. In particular, we note that the X states, although evanescent, are highly excited, contributing a larger part of the overall charge density than the only propagating, L state(). The evanescent X states are also responsible for a considerable fraction of the total current [Figs. 6(d) and 6(e)]. Extrema of minibands with "anomalous" dispersion, being inside the superlattice Brillouin zone, are characterized by two large X and L state current counterflows that cancel at the exact extremum point, underlining again the strength of the L-X mixing. In contrast, the current at $k_{SL}=0$ vanishes because all the current components vanish. The wave function and the total current [even slightly off the exact extrema, at $k_\varepsilon \to 0$] have very different compositions in the two halves of the superlattice period, which is very clearly seen here, but is also noticeable in Si superlattices [Fig. 5(b)]. This is caused by the asymmetry of the underlying single-layer bulk dispersion. At $-k_\varepsilon$, the wave functions and currents displayed in Figs. 6(d) and 6(e) are reversed.

Germanium-based twinning superlattices with $m \neq n$ are qualitatively similar to Si-based ones, except that X-L mixing is again much more pronounced. From the examples given in Fig. 7 one can see that these superlattices, *unlike any conventional superlattices,* may have indirect mini band gaps. Furthermore, the envelope wave-

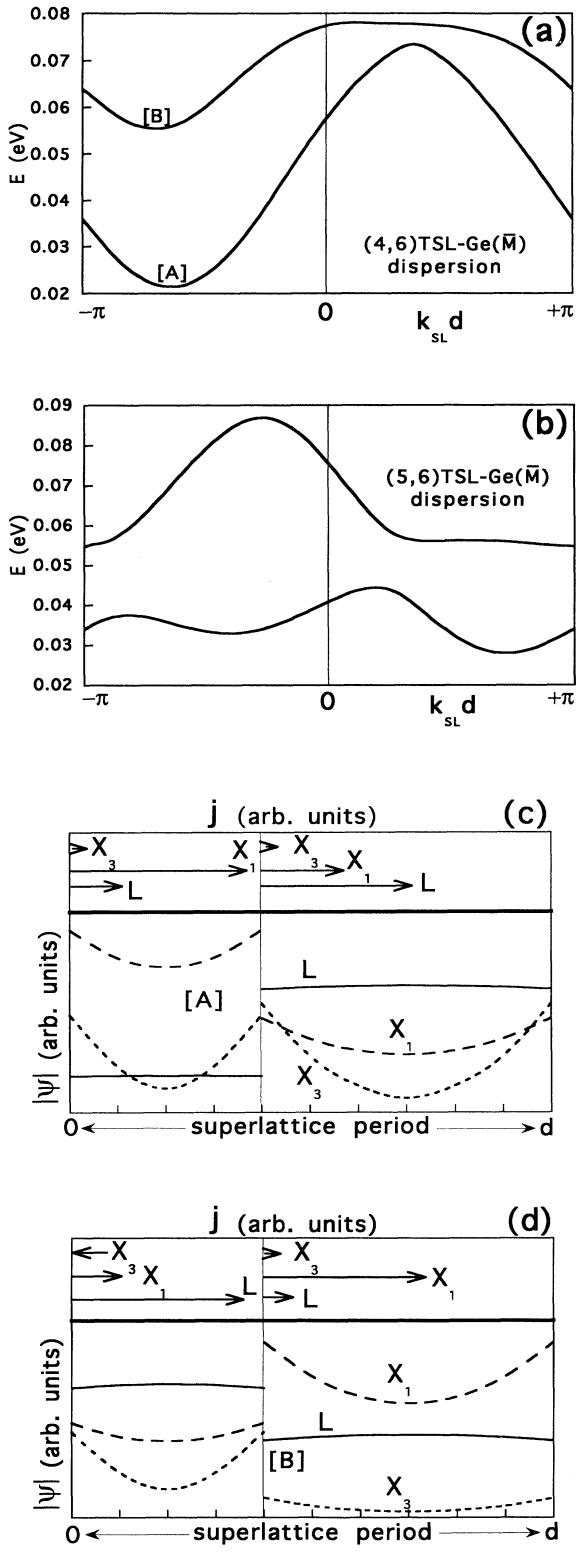

FIG. 7. (a) and (b) Dispersion of the lowest two minibands in (4,6) and (5,6) Ge twinning superlattices at the $\bar{M}$ point of the interface Brillouin zone. (c) and (d) Envelope wave functions and current components at points [A] and [B] in the (4,6) twinning superlattice.

function components, as well as current components, are now grossly discontinuous. Discontinuity of different bulk states at the interface applies to some extent in any superlattice, but in Ge-based twinning superlattices at the $\bar{M}$ point this effect is drastic because, as discussed above, states in one layer have no direct match in the other layer, as a consequence of the 180° rotation, and at the same time they are very close in energy, allowing for substantial mixing. A similar situation can also be found in conventional type-II superlattices, e.g., GaSb/InAs, where conduction-band and valence-band bulk states both contribute to the superlattice state, due to the appropriate band alignment, and the component bulk states are highly discontinuous at the interface.

In GaAs-, or AlAs-based twinning superlattices at the $\bar{M}$ point, no essentially new features appear that have not already been discussed. Thus, e.g., the miniband structure of the GaAs (n,n) superlattice looks very much the same as in Ge, except that the "anomalous" dispersion continues to higher energies than is the case in Ge, i.e., minibands III and IV also show this feature for larger n values.

2. $\bar{\Gamma}$ point

At the $\bar{\Gamma}$ point of the interface Brillouin zone, as discussed in Sec. II, it will be the bulk L and Γ states that take part in forming the twinning-superlattice miniband structure. However, the Γ-L mixing is not expected to be very large, especially not in Si. On the other hand, a feature that was absent at the $\bar{M}$ point—the existence of bound states or resonances—will here take part in miniband formation.

The calculated miniband structure of twinning superlattices at the $\bar{\Gamma}$ point of the interface Brillouin zone for (n,n) twin stacking-fault superlattices made of Si and of Ge are shown in Figs. 8(a) and 8(b), respectively. There is a lot of similarity between the two materials now, in spite of the fact that the Γ-L separation in Si is very much larger than the one in Ge. The only real difference between the two is that the minibands in Si-based superlattices are ~ 1 eV above those at $\bar{M}$, and thus will not have a large influence on most electronic and optical properties of these structures. The miniband structure of the corresponding Ge-based superlattices is set at lower energies. Since bulk Ge is an L-type indirect-gap semiconductor, the minibands at both the $\bar{\Gamma}$ and $\bar{M}$ points have energies in the same range, and are therefore equally important and experimentally accessible.

The most important point to note here is the existence of minibands derived from bound (evanescent) states, partly or fully below the bulk conduction-band edge at the $\bar{\Gamma}$ point. As the superlattice period increases, these minibands collapse into the single twin stacking-fault bound state from which they originate [Figs. 2(a) and 2(b)]. The energy range spanned by these minibands is at least partly (fully for longer periods, $n \geq 6$) below the lowest conduction-band edge (i.e., L valley) at this point of the interface Brillouin zone, and in such cases the corresponding wave functions clearly cannot contain any propagating bulk state. Yet, due to the periodicity of the

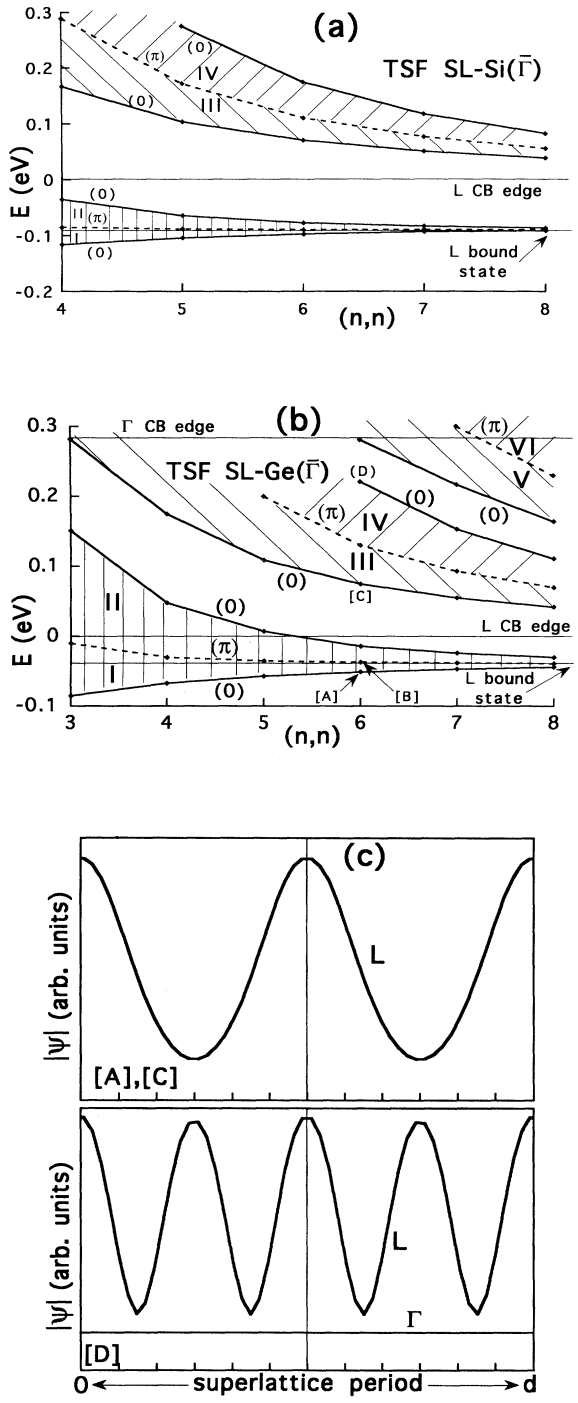

FIG. 8. (a,b) Miniband structure of the (a) Si-based and (b) Ge-based (n,n) twin stacking-fault superlattice at the $\bar{\Gamma}$ point of the interface Brillouin zone. The energy is measured from the conduction-band edge at $\bar{\Gamma}$, which coincides with the bulk L-valley bottom. The notation is the same as in Fig. 5. (c) Envelope wave functions at a couple of characteristic points, denoted in (b) (the situation in $[B]$ is similar to that in $[A]$ and $[C]$ and is not separately displayed). Whether evanescent or propagating, only the bulk L states here contribute significantly to the superlattice state.

twin boundary array, they are of Bloch type. This is, to our knowledge, the only superlattice with some of its minibands formed *entirely* from the evanescent bulk states. The nearest analog are the interface phonon bands found in the GaSb-InAs superlattice.[34]

Minibands arising from the interface states exhibit almost purely L character (Γ-L mixing is very low). The miniband wave functions are then composed of pairs of growing and decaying evanescent L states, an admixture of Γ being significant for higher energies only. In the corresponding energy range the current is also entirely carried by coupled pairs of evanescent states. The wave-function plots, given in Fig. 8(c), show that for lower-lying minibands, they tend to be piled up at interfaces (this holds true even at energies higher than the L-valley edge), but for higher minibands, additional peaks of the wave function appear inside the layers.

In III-V-semiconductor-based twinning superlattices (GaAs, AlAs) the situation is rather similar to that in group-IV-based ones. Consider first the GaAs (n,n) superlattice at $\bar{\Gamma}$: since the Γ valley in bulk material is the lowest, the first miniband, which is predominantly Γ in character, has its bottom only slightly elevated from the bulk conduction-band edge and is extremely broad (Fig. 9). This is consistent with the fact that electron transmission at the $\bar{\Gamma}$ point is almost equal to unity for energies exceeding a couple of meV. Immersed in this Γ miniband are the pair of interface-resonance-related minibands, which are essentially L in character. Somewhat higher, above the L conduction-band edge, but also inside the broad Γ miniband, is an L-valley-related miniband.

Finally, AlAs-based twinning superlattices do not show any new features other than those already discussed above. At the $\bar{\Gamma}$ point the miniband structure is similar to that of Si or Ge, and at $\bar{M}$ to that of GaAs (although its X and L valleys are oppositely ordered), displaying the "anomalous dispersion" phenomena in the lowest two miniband pairs. As an example of the electronic structure in this case, we give the lowest four minibands at the $\bar{\Gamma}$ point of AlAs-based $(n,6)$ twinning superlattice with

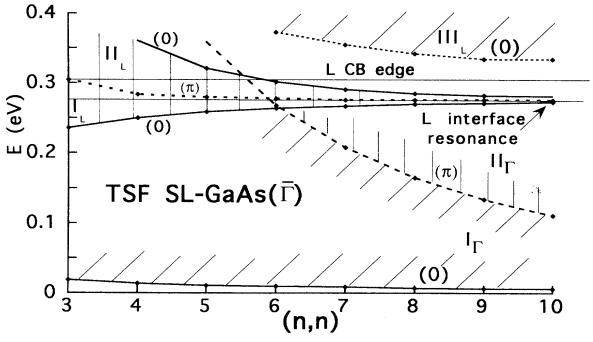

FIG. 9. Miniband structure of the GaAs-based (n,n) twin stacking-fault superlattice at the $\bar{\Gamma}$ point of the interface Brillouin zone, from which the energy is measured (the bulk Γ-valley bottom). The notation is the same as in Fig. 5(a). Since two kinds of minibands are present, they are denoted by the corresponding subscript, according to their character (Γ or L).

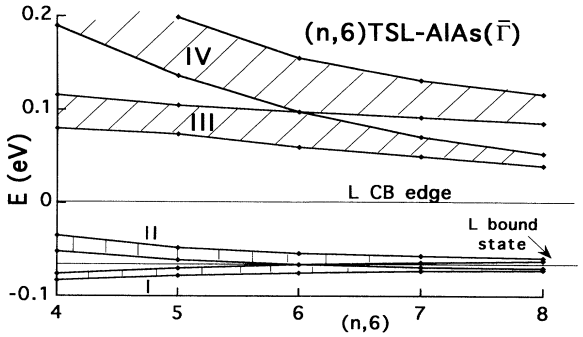

FIG. 10. Miniband structure of the AlAs-based $(n,6)$ twinning superlattice at the $\bar{\Gamma}$ point of the interface Brillouin zone, from which the energy is measured (the bulk L-valley bottom). Note the coalescence of the lowest miniband pair (i.e., the appearance of a zero energy gap) for $n=6$.

$4 \leq n \leq 8$ in Fig. 10. Coalescence of miniband pairs at $n=6$ may be clearly seen.

IV. DISCUSSION

As a summary of the results presented above, we note that interminiband separation in twinning superlattices is in the 100-meV range, similar to that observed in their conventional counterparts. The miniband electron effective masses are also in the range obtained for conventional superlattices. As an example, the effective masses (in free-electron mass units) of the lowest miniband of Si-based (n,n) superlattices at the $\bar{M}$ point are $m=1.18$ for (3,3), $m=1.50$ for (4,4), $m=0.47$ for (5,5), and $m=0.86$ for (6,6) superlattices, respectively (note that the values oscillate between the even-even and odd-odd cases; see, for example, Fig. 5(a). In $(n,1)$ intrinsic stacking-fault superlattices [Fig. 4(a)] the lowest miniband masses are $m=2.0$ for (3,1), $m=0.73$ for (5,1), $m=0.53$ for (6,1), and $m=0.41$ for (8,1). Thus, miniband parameters that are normally generated by the built-in potential in conventional superlattices may also be obtained by the interface scattering alone in twinning superlattices.

We should also note that, unlike the conventional heterostructures, twinning alone cannot be used for making single quantum wells, since it does not have the asymptotic binding properties that confining potentials have (actually, twinning superlattices may behave as barriers for electron energies corresponding to their stop bands, but the usefulness of such an application is rather dubious.) However, if combined with the classical heterostructure quantum well, e.g., by making twin boundaries coincident with heterointerfaces, twinning might provide a means of barrier "wall hardening," especially for bound states not too high in energy. This would primarily be of use in Si-(SiGe) systems where the conduction bands are entirely X derived [but certainly not for Γ-valley electrons, e.g., in GaAs-(AlGa)As and similar systems, for which the twinning boundary is almost fully transparent].

As mentioned in the Introduction, we are not presently aware of any experiment in growing twinning superlattices. This, however, should not be discouraging, since

the technology has been mostly directed towards the reduction of the number of defects in growing various microstructures, and not in the enhancement of their production. As for the single stacking faults, it is well known that they may be found in stress deformed monocrystals, not only in Si but in III-V crystals as well,[35] and may have quite large areas. However, this method is probably too crude for making superlattices. There has also been a report[36] on fabrication of a single low angle twist boundary in Si that in principle allows for making multiple stacking faults, but it is not certain if the method could be extended to growing ultrathin layer structures. One approach, at least for some classes of twinning superlattices, might include the application of indentation technique, used by Pirouz *et al.*[37] Other, perhaps somewhat speculative and naive, ideas would include the application of an appropriate stress (adjustable in direction and magnitude) during the crystal growth and/or—in the case of semiconductors with some amount of ionicity—an electric field[38] that would favor particular stacking sequences. The most encouraging report, however, is on the successful (homoepitaxial) growth of twinning boundary (twin stacking fault) in silicon, with the help of boron-submonolayer-induced surface reconstruction.[11] The method seems very promising, and might, in our opinion, be extended towards growing twinning superlattices. As noted in Ref. 11, the role of boron is only temporary, and once the twinning boundary is made, it can be removed and/or compensated by some other dopant.

Another point to discuss is the stability of twinning superlattices. Due to the positive formation energies of stacking faults, these superlattices would be essentially metastable structures. It may turn out that those with very low (m,n) indices are not sufficiently stable to really exist under normal conditions (similar problems may occur in polytype superlattices).[7] However, in the case of larger (m,n) values, the energetically favorable single or multiple $AA'BB'CC'$ sequences of diamond-type and zincblende-type structure may be found within a superlattice period, and such superlattices should be sufficiently (meta)stable, just as are single stacking faults or twins that, once made, show no tendency to relax to energetically more favorable perfect crystal. The special case of an (n,n) twinning superlattice may in principle show an additional instability, known to occur in polyacetylene molecular chains. Since the polyacetylene molecule also has the screw symmetry, as does the (n,n) twinning superlattice, it turns out that the electronic pressure makes it "reconstruct," so as just to remove the screw symmetry and lower the Fermi level.[32] Yet, this need not happen in (n,n) twinning superlattices—for instance, hcp zirconium bulk crystal, where such a possibility also exists, really shows no tendency towards reconstruction.[32] Specifically, some preliminary physical considerations indicate that undoped or lightly doped twinning superlattices are stable, but very heavily doped ones might undergo Peierls reconstruction. These problems, however, can only be investigated by making total-energy calculations, analogous, e.g., to those in Refs. 2–5, and are beyond the scope of this paper.

V. CONCLUSION

The electronic structure of single stacking faults and the recently proposed twinning superlattices were analyzed within the empirical-pseudopotential framework. As one can see from the results presented, twinning superlattices would offer almost as much versatility in tailoring the electronic miniband structure as there exists in ordinary heterostructure-based superlattices. Certainly the two principles of building the superlattice periodicity (crystal orientation and material composition or doping) may be combined to extend the possibilities of "band-structure engineering" even more, once the means of fabricating twinning superlattices are devised. In view of the recent advances[11] in fabricating a high-quality single twin boundary, which is the elementary "building block" of twinning superlattices, we may expect this to occur quite soon.

ACKNOWLEDGMENTS

The authors would like to thank the SERC (UK) for computational facilities through the CSI scheme. One of the authors (Z.I.) is grateful to the Royal Society and SERC (UK) for financial support.

[1]S. Yoshida, E. Sakuma, H. Okumura, S. Misawa, and K. Endo, J. Appl. Phys. **62**, 303 (1987).
[2]C.-Y. Yeh, Z. W. Lu, S. Froyen, and A. Zunger, Phys. Rev. B **46**, 10 086 (1992).
[3]A. Qteish, V. Heine, and R. J. Needs, Phys. Rev. B **45**, 6534 (1992).
[4]G. E. Engel, J. Phys. Condens. Matter **2**, 6905 (1990).
[5]G. E. Engel and R. J. Needs, J. Phys. Condens. Matter **2**, 367 (1990).
[6]G. B. Dubrovskii and A. A. Lepneva, Fizi. Tverd. Tela (Leningrad) **19**, 1252 (1977) [Sov. Phys. Solid State **19**, 729 (1977)].
[7]M. Murayama and T. Nakayama, J. Phys. Soc. Jpn. **61**, 2419 (1992); Superlatt. Microstruct. **12**, 215 (1992).
[8]M. D. Stiles and D. R. Hamann, Phys. Rev. B **38**, 2021 (1988).
[9]M. D. Stiles and D. R. Hamann, Phys. Rev. B **41**, 5280 (1990).
[10]Z. Ikonić, G. P. Srivastava, and J. C. Inkson, Solid State Commun. **86**, 799 (1993).
[11]R. L. Headrick, B. E. Weir, J. Bevk, B. S. Freer, D. J. Eaglesham, and L. C. Feldman, Phys. Rev. Lett. **65**, 1128 (1990).
[12]J. P. Stark, Phys. Rev. B **38**, 1139 (1988).
[13]C. A. Sorrel and G. F. Sandstrom, *The Rocks and Minerals of the World* (Collins, London, 1977).
[14]L. V. Azaroff, *Introduction to Solids* (McGraw-Hill, New York, 1960).
[15]P. J. Born, D. S. Robertson, P. W. Smith, and I. M. Young, J. Mater. Sci. Lett. **6**, 635 (1987).
[16]L. J. Chen and L. M. Falicov, Philos. Mag. **29**, 1 (1974).
[17]E. Chacon, C. Tejedor, and F. Flores, Phys. Status Solidi B **98**, K117 (1980).
[18]S. Marklund, Phys. Status Solidi B **108**, 97 (1981).

[19]L. F. Mattheiss and J. R. Patel, Phys. Rev. B **23**, 5384 (1981).
[20]J. Sanches-Dehesa, J. A. Verges, and C. Tejedor, Phys. Rev. B **24**, 1006 (1981).
[21]M. Y. Chou, M. L. Cohen, and S. G. Louie, Phys. Rev. B **32**, 7979 (1985).
[22]Z. Zhao-Bo and L. Jin-Ling, J. Phys. C **19**, 6739 (1986).
[23]A. Gross and H. Teichler, Philos. Mag. B **64**, 413 (1991).
[24]H. Bross, J. Phys. F **12**, 2883 (1982).
[25]B. Hammer, K. W. Jacobsen, V. Milman, and M. C. Payne, J. Phys. Condens. Matter **4**, 10 453 (1992).
[26]A. F. Wright, M. S. Daw, and C. Y. Fong, Philos. Mag. A **66**, 387 (1992).
[27]D. Y. K. Ko and J. C. Inkson, Phys. Rev. B **38**, 9945 (1988).
[28]Z. Ikonić, G. P. Srivastava, and J. C. Inkson, Phys. Rev. B **46**, 15 150 (1992).
[29]J. R. Chelikowsky and M. L. Cohen, Phys. Rev. B **14**, 556 (1976).
[30]M. L. Cohen and T. K. Bergstresser, Phys. Rev. **141**, 789 (1966).
[31]E. Caruthers and C.-L. Chung, Phys. Rev. B **17**, 2705 (1978).
[32]S. L. Altmann, *Band Theory of Solids: An Introduction from the Point of View of Symmetry* (Clarendon, Oxford, 1991).
[33]V. Milanović and Z. Ikonić, Phys. Rev. B **37**, 7125 (1988).
[34]Y. Liu and J. C. Inkson, Semicond. Sci. Technol. **6**, 335 (1991).
[35]A. Lefebvre, Y. Androussi, and G. Vanderschaeve, Philos. Mag. Lett. **56**, 135 (1987).
[36]G. C. Perreault, S. L. Hyland, and D. G. Ast, Philos. Mag. A **64**, 587 (1991).
[37]P. Pirouz, R. Chaim, U. Dahmen, and K. H. Westmacott, Acta Metall. Mater. **38**, 313 (1990).
[38]B. Palosz and J. Przedmojski, Cryst. Res. Technol. **17**, 1513 (1982).